Environmental Research Letters

LETTER

Compensatory climate effects link trends in global runoff to rising atmospheric CO_2 concentration

Hui Yang[1,2], **Chris Huntingford**[1], **Andy Wiltshire**[3], **Stephen Sitch**[4] and **Lina Mercado**[4,1]

[1] Centre for Ecology and Hydrology, Benson Lane, Wallingford OX10 8BB, United Kingdom
[2] Sino-French Institute for Earth System Science, College of Urban and Environmental Sciences, Peking University, Beijing 100871, People's Republic of China
[3] Met Office Hadley Centre, Exeter, United Kingdom
[4] College of Life and Environmental Sciences, University of Exeter, Exeter, United Kingdom

E-mail: yang_hui@pku.edu.cn

Keywords: runoff, climate change, atmospheric CO_2, hydrological cycle, carbon–nitrogen interaction

Supplementary material for this article is available online

OPEN ACCESS

RECEIVED
26 July 2019

REVISED
29 October 2019

ACCEPTED FOR PUBLICATION
27 November 2019

PUBLISHED
18 December 2019

Abstract

River runoff is a key attribute of the land surface, that additionally has a strong influence on society by the provision of freshwater. Yet various environmental factors modify runoff levels, and some trends could be detrimental to humanity. Drivers include elevated CO_2 concentration, climate change, aerosols and altered land-use. Additionally, nitrogen deposition and tropospheric ozone changes influence plant functioning, and thus runoff, yet their importance is less understood. All these effects are now included in the JULES-CN model. We first evaluate runoff estimates from this model against 42 large basin scales, and then conduct factorial simulations to investigate these mechanisms individually. We determine how different drivers govern the trends of runoff over three decades for which data is available. Numerical results suggest rising atmospheric CO_2 concentration is the most important contributor to the global mean runoff trend, having a significant mean increase of $+0.18 \pm 0.006$ mm yr^{-2} and due to the overwhelming importance of physiological effects. However, at the local scale, the dominant influence on historical runoff trends is climate in 82% of the global land area. This difference is because climate change impacts, mainly due to precipitation changes, can be positive (38% of global land area) or negative (44% of area), depending on location. For other drivers, land use change leads to increased runoff trends in wet tropical regions and decreased runoff in Southeast China, Central Asia and the eastern USA. Modelling the terrestrial nitrogen cycle in general suppresses runoff decreases induced by the CO_2 fertilization effect, highlighting the importance of carbon–nitrogen interactions on ecosystem hydrology. Nitrogen effects do, though, induce decreasing trend components for much of arid Australia and the boreal regions. Ozone influence was mainly smaller than other drivers.

1. Introduction

Climate change, direct human activity and perturbed biogeochemical cycles are rapidly altering the hydrological cycle (Milly *et al* 2005, Huntington 2006). River runoff is a key component of the hydrological cycle, providing a robust metric of freshwater availability to humans and ecosystems (Oki and Kanae 2006). However, uncertainties exist in drivers of runoff variability, preventing a better understanding and quantification of spatio-temporal distributions of freshwater provision (Yang *et al* 2017). To reduce such uncertainty, the careful merging of measurements and models needs to continue. The knowledge gained enables the hydrological community to support adaptation and mitigation strategies for climate change and related sustainable management (Jiménez Cisneros *et al* 2014). In particular, better understanding increases capacity to perform more accurate projections of future runoff.

Multiple environmental factors cause variations in runoff, that can be both different in sign and magnitude, and show high local variability (e.g. Huntingford *et al* 2011). First, runoff is driven by climatic variables, which we call 'CLIM' forcings, and these include

precipitation amount and intensity, temperature, wind speed, and radiation. Both precipitation amount and intensity play a direct critical role in runoff generation (Xue and Gavin 2008, Berghuijs *et al* 2014). Temperature, wind speed and radiation influence evapotranspiration, in turn affecting runoff. Moreover, global warming impacts vegetation growth via altered photosynthesis, plant respiration and phenology, which again influences runoff via evapotranspiration and interception changes (Ohmura and Wild 2002, McVicar *et al* 2012). Second, atmospheric CO_2 concentration impacts runoff variability in two compensatory ways. Increased CO_2 concentration leads to reductions in stomatal conductance, increasing plant water use efficiency (WUE), thus reducing evapotranspiration and increasing runoff (Gedney *et al* 2006). However, enhanced vegetation growth, via increased leaf area index (LAI) and extended growing seasons, increases evapotranspiration, so causing a decline in runoff. High LAI systems are likely to be dominated by the WUE effect, while in low LAI systems, the CO_2 effect on WUE and LAI might counteract (Piao *et al* 2007). These two combined effects are named 'CO2'. Third, terrestrial nitrogen availability limits the CO_2 fertilization effect, and thus affecting runoff. An earlier analysis using the O-CN model, which accounts for the interactions between the terrestrial carbon and nitrogen cycles, suggests that the effect of CO_2 fertilization on carbon sequestration could be constrained by up to 70% when compared to only modelling the carbon cycle (Zaehle 2013); such carbon–nitrogen interactions would also impact runoff. Additionally, atmospheric nitrogen deposition, mainly occurring in the mid and high northern latitudes, could alleviate plant growth suppression in otherwise nitrogen limited systems. This may increase evapotranspiration and decrease runoff (Shi *et al* 2011, Mao *et al* 2015). These effects, we term 'CN&NDE'. Fourth, land use change ('LUC') alters canopy interception, land surface albedo, soil infiltration, and evapotranspiration, all of which can result in runoff changes (Mahmood and Hubbard 2003). Fifth, increases in atmospheric aerosols ('AER') can enhance plant photosynthesis via increased diffuse radiation conditions (Mercado *et al* 2009), and alter the water balance of ecosystems with associated changes in evapotranspiration and runoff (Gedney *et al* 2014). Sixth, tropospheric ozone ('O3') affects plant stomata and reduces photosynthetic rates, likely reducing transpiration rate and enhancing runoff (Sitch *et al* 2007, Felzer *et al* 2009, Lombardozzi *et al* 2015, Mills *et al* 2016, Oliver *et al* 2018).

Recent research has improved the understanding of the individual factors that control runoff variability. Yet the comparison of the relative magnitudes of the different mechanisms and factors that govern long-term trends of runoff, across scales, are poorly quantified. We provide a comprehensive local and global assessment of the balance among the contributions of the six environmental factors (i.e. CLIM, CO_2, LUC, CN&NDE, AER and O3). We analyse changes to trends in global and local runoff over recent decades, based on the JULES-CN model. The previous standard JULES-C model, without terrestrial carbon–nitrogen interactions, has been used in many studies including benchmarking against a range of datasets (Blyth *et al* 2011), and detection and attribution analyses of runoff changes (Gedney *et al* 2006, Zulkafli *et al* 2013, Gedney *et al* 2014). The main advance here is to investigate refined estimates of runoff changes, enabled by a common modelling framework that now additionally includes interactions between the carbon and nitrogen cycles, and with tropospheric ozone impacts.

2. Data, modelling framework and factorial simulations

2.1. Runoff data

Observed monthly river discharge records, for years 1960–1999 inclusive, are used for JULES-CN model evaluation. Discharge measurements are from the farthest downstream stations, and for 42 large basins around the world (figure S1 is available online at stacks.iop.org/ERL/14/124075/mmedia). These are obtained from three sources: (i) Global River Discharge Centre (http://bafg.de/GRDC); (ii) China Statistical Yearbook (Bureau 2000); and (iii) river discharge archive by Dai *et al* (2009). The two main selection criteria for catchments are they need to have >80% available data for the study period, and catchment areas are >100 000 km^2 to match the relatively large spatial resolution (gridbox of 1.25° lat × 1.875° lon, ~60 000 km^2) used in the JULES-CN simulations of this study.

2.2. Modelling framework

The Joint UK Land Environment Simulator (JULES; Best *et al* 2011, Clark *et al* 2011) is the land surface scheme of the UK Met Office Earth System Model. JULES can also be operated 'offline', as here, and forced with known surface meteorological conditions for the contemporary period. JULES evolved from the Met Office Surface Exchange Scheme (MOSES; Cox *et al* 1998, 1999), combined with a dynamic vegetation module called the Top-down Representation of Interactive Foliage and Flora Including Dynamics (TRIFFID; Essery *et al* 2003, Clark *et al* 2011). The current JULES version contains a sophisticated representation of canopy radiation interception (Mercado *et al* 2007) that defines explicitly the diffuse and direct components of the photosynthetically active radiation (Mercado *et al* 2009). It also includes a representation of the response of vegetation to tropospheric ozone deposition (Sitch *et al* 2007).

Notably, JULES-CN has implemented the nitrogen cycle into the dynamic global vegetation and

Table 1. Initial factorial simulations with JULES-C and JULES-CN. Driving factors include rising CO_2, climate change, land use/land cover change, carbon–nitrogen interaction and nitrogen deposition. Factors changing over the transient period have the '√' symbol and factors that are fixed at the pre-industrial levels have no symbol.

Model	Simulation	CO_2	CLIM	LUC	CN&NDE
JULES-C	C_{ctrl}				
	C_{CO2}	√			
	$C_{CO2+CLIM}$	√	√		
	$C_{CO2+CLIM+LUC}$	√	√	√	
JULES-CN	$CN_{ctrl+CN\&NDE}$				√
	$CN_{CO2+CN\&NDE}$	√			√
	$CN_{CO2+CLIM+CN\&NDE}$	√	√		√
	$CN_{CO2+CLIM+LUC+CN\&NDE}$	√	√	√	√

Table 2. Second factorial simulations, including atmospheric aerosols and tropospheric O_3 concentration effects. The symbol '√' means factors are changing over the transient period, while factors that are fixed at the pre-industrial levels and conditions have no symbol. Simulation $CN_{CO2+CLIM+LUC+CN\&NDE}$ is identical between the tables 1 and 2.

Simulation	CO2	CLIM	LUC	CN&NDE	AER	O3
$CN_{CO2+CLIM+LUC+CN\&NDE}$						
$CN_{CO2+CLIM+LUC+CN\&NDE+AER}$			√		√	
$CN_{CO2+CLIM+LUC+CN\&NDE+O3}$						√

hydrology components of the JULES model (Wiltshire *et al* 2019). In particular, processes of soil nitrogen dynamics, litter production, plant uptake, nitrogen allocation, response of photosynthesis and maintenance respiration to varying nitrogen concentrations in plant organs and inorganic nitrogen are now included in the model. This addition improves the simulation of vegetation distribution, as it responds to climate, CO_2 and nutrient availability. This new JULES framework also allows an assessment of the impacts of vegetation carbon–nitrogen interactions on hydrological processes, including those driven by changing atmospheric nitrogen deposition. In brief, the nitrogen module acts to reduce Gross Primary Productivity (GPP) in regions where insufficient inorganic nitrogen exists to meet demand. In regions of nitrogen limitation, it is expected that the vegetation biomass and leaf area will be less stimulated under raised atmospheric CO_2 concentrations, compared to the model version without nitrogen representation (i.e. JULES-C). The effect of nitrogen is to generally cause altered vegetation structure, as opposed to changes to stomatal conductance. Inorganic sources of nitrogen include deposition, fixation and soil net mineralization, and in some circumstances, these offset nitrogen limitation.

2.3. Simulation setup

We run two sets of simulations: one using the JULES model with carbon–nitrogen interactions (JULES-CN) and one without carbon–nitrogen interactions (JULES-C). Such simulations, named 'factorial', isolate the individual contributions of elevated CO_2 concentration, climate change and LUC predicted by JULES-C and JULES-CN models (table 1). Here, JULES-C and JULES-CN simulate historical land surface conditions, driven by a 99 year (1901–1999) observation-based meteorological forcing dataset, CRU-NCEP v4 (Le Quéré *et al* 2012). In addition, annual atmospheric CO_2 concentration data is from Keeling and Whorf (2005), LUC data from the HYDE dataset (Klein Goldewijk 2011) and nitrogen deposition from ACCMIP (Lamarque *et al* 2013). All simulations are 'spun up' to equilibrium (i.e. at 1901) under environmental conditions by a repeated 20 year climate forcing data (1901–1920) and fixed pre-industrial values of CO_2, land-use and nitrogen deposition.

Comprehensive global observations of diffuse and direct partitioning of downward shortwave radiation and ozone concentrations are unavailable. The simulations in table 1 use the fixed diffuse fraction of 0.4 and the pre-industrial O_3 concentration. To assess O_3 and aerosol radiative effects on runoff changes, we add an extra second set of two JULES-CN simulations (table 2). We use HadGEM2-based estimates of diffuse fraction and O_3 concentration, and combine with the same estimates of surface meteorological conditions that are used for the simulations in table 1 as the forcing. The radiative effects of atmospheric aerosols adjust the balance of downward shortwave between direct and diffuse levels. Here, the aerosol forcing data, similar to Mercado *et al* (2009), includes tropospheric aerosol species: black carbon, sulphate, mineral dust, sea salt and biomass burning. Distributions of aerosol optical depths for each species were simulated by the atmospheric model in HadGEM2-A, following Bellouin *et al* (2007). Radiative transfer calculations

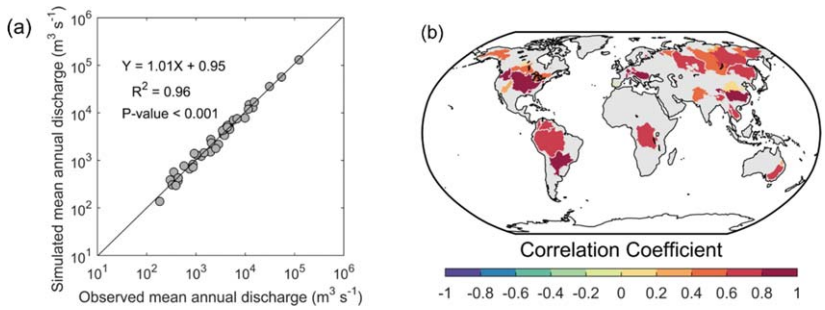

Figure 1. Assessment of model performance. (a) Comparison of mean annual river discharge measured at gauging stations versus that simulated by the JULES-CN model with all forcings ($CN_{CO2+CLIM+LUC+CN\&NDE+AER}$ simulation + O3 effects). (b) A map of Pearson correlation coefficients of modelled annual river discharge (again, from $CN_{CO2+CLIM+LUC+CN\&NDE+AER}$ simulation + O3 effects) with the measured river discharge time series.

are used to estimate diffuse fraction at the land surface, based on these aerosol distributions, which surface level is input to JULES (Mercado *et al* 2009). The tropospheric ozone forcing data, similar to Sitch *et al* (2007), is generated by 'time-slice' simulations with a tropospheric chemistry model STOCHEM (Sanderson *et al* 2003). Values for the intermediate years are generated by linear interpolation.

2.4. Scale dependence of relative dominant factors

To illustrate how the dominant drivers vary with spatial scale, we follow the method used by Jung *et al* (2017) and define the relative magnitudes of environmental components ('COMP') that force runoff trends. This metric is defined as the trend of runoff forced by an individual component, divided by the trends of runoff forced by all factors ($trend_{ALL}$): $D^{COMP} = |trend_{COMP}|/|trend_{ALL}|$. This index is calculated for spatial windows of 1×1, $2 \times 2, 4 \times 4, 8 \times 8, 16 \times 16, 28 \times 32, 56 \times 48$, and all the grid cells over the globe. The magnitude of spatial scales (in km) defined by the longitudinal distance at 45°N is also shown in figure 7.

3. Results

3.1. Evaluation of simulated present-day runoff

We first evaluate the JULES model performance in reproducing historical river discharge for period 1960–1999 (figure 1). The JULES-CN model performs well in capturing the long-term averages of annual discharge (figure 1(a)) and the inter-annual variability of annual discharge (figure 1(b)) for the 42 major basins, and for the period 1960–1999, when the effects of all six forcings are included.

The JULES-CN model performs well for many basins e.g. Congo, Mississippi and Yangtze. However, it has a limited ability to reproduce observed runoff increases in a few basins, e.g. some Eurasian Arctic rivers, the Amazon and Pakistan basins. Increased precipitation plays a major role in observed Eurasian river discharge increases, but poor performance there could be partly related to the uncertainty in regional precipitation. For instance, the NCEP precipitation data shows smaller increases than other precipitation datasets in high latitudes (a point also noted in Pavelsky and Laurence 2006). In addition, these Eurasian Arctic rivers are highly affected by permafrost (figure S2), which as yet is not fully included in JULES-CN. The bias in trends for Asian basins may reflect poor representation of direct human intervention (notably dams, irrigation) on runoff (Yang *et al* 2018). Raised levels of irrigation and regulation enhance surface evaporation and possibly reduce runoff in intensively cultivated areas (hence our findings support those of Tang *et al* 2007, Haddeland *et al* 2014). In the Amazon basin, the model-data discrepancy might be partly related to an inadequate representation of the response to land use, notably deforestation.

There are strong similarities between figures 2(b)–(d), providing initial evidence that AER and O3 effects are likely relatively small drivers.

3.2. Global runoff trends and factor contributions

Annual global runoff averages are calculated from the 42 large river basins (figure S1), for comparison with observations. The time-evolving, observation-based global average of runoff has a small (but statistically significant) positive trend of $+0.22 \pm 0.20$ mm yr^{-2} ($+0.07 \pm 0.06\%$ yr^{-1}) during the period of 1960–1999 (figure 3(a)). The JULES-CN simulation $CN_{CO2+CLIM+LUC+NDE}$ provides a comparable estimate of the global runoff trend of $+0.30 \pm 0.27$ mm yr^{-2}.

Further analyses use the factorial simulations to quantify the contributions of six environmental factors to the global averages of modelled runoff linear trends for the period of 1960–1999 (figure 3). Values are also calculated from the 42 large study basins, and are first presented as the accumulation of each factor (yellow bars, figure 3), before showing the isolated effects of the individual drivers. Contributions from changing climate are small for the large-scale averages (just $+0.01 \pm 0.30$ mm yr^{-2}). Rising atmospheric CO_2 concentration is the most important contributor to the global river runoff trend, with a significant increase of $+0.18 \pm 0.006$ mm yr^{-2}. Important

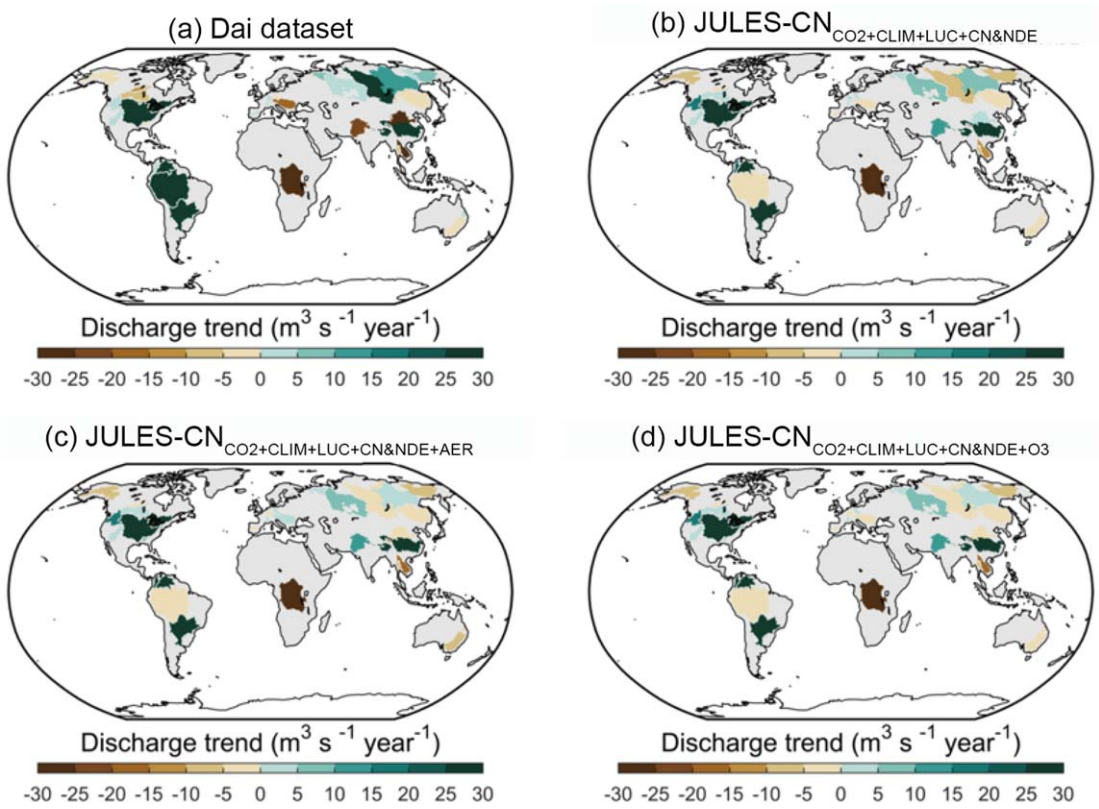

Figure 2. Runoff trends from 1960 to 1999 for the 42 major basins. Runoff trends are estimated from the Dai river runoff dataset (a), and from JULES-CN simulations under (b) $CN_{CO2+CLIM+LUC+CN\&NDE}$ (c) $CN_{CO2+CLIM+LUC+CN\&NDE+AER}$ and (d) $CN_{CO2+CLIM+LUC+CN\&NDE+O3}$. (b) has driving factors of CO_2, CLIM, LUC and CN&NDE. (c) is the same as (b), but with AER added. (d) is the same as (b), but with O3 added.

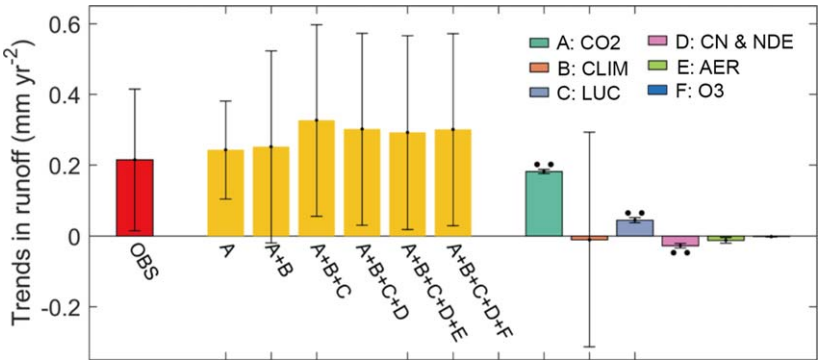

Figure 3. Global averages of observed (red) and modelled runoff linear trends (yellow, represents the factorial simulations) for the period of 1960–1999. Global averages are calculated from the river basins used in the study only. Modelled runoff changes due to the single effects of elevated CO_2 concentration (A: CO_2), climate change (B: CLIM), land use change (C: LUC), carbon–nitrogen interactions and nitrogen deposition (D: CN&NDE), aerosol radiative effects (E: AER) and tropospheric ozone changes (F: O3). Error bars show one standard error of the regression coefficients. Two dots indicate that the trend is statistically significant ($P < 0.10$).

contributions are also LUC (increase in total runoff of $+0.05 \pm 0.007$ mm yr^{-2}) and carbon–nitrogen interactions and nitrogen deposition (decrease of -0.03 ± 0.007 mm yr^{-2}). The radiative effects of atmospheric aerosols adjusting the balance of downward shortwave between direct and diffuse levels, and ozone concentration changes, both exert a slightly negative influence on global runoff changes. Thus, there are no significant differences among the globally-averages of runoff change between $CN_{CO2+CLIM+LUC+CN\&NDE}$, $CN_{CO2+CLIM+LUC+CN\&NDE+AER}$ and $CN_{CO2+CLIM+LUC+CN\&NDE+O3}$ simulations, supporting the noted small effects on global runoff trends of aerosol and O3 forcings (figures 2(b) versus (c) and (d)).

3.3. Local runoff trends and contribution from environmental factors

Figure 3 shows at global scale, almost all drivers have relatively little effect on runoff trends, except for increasing atmospheric CO_2. However, the findings

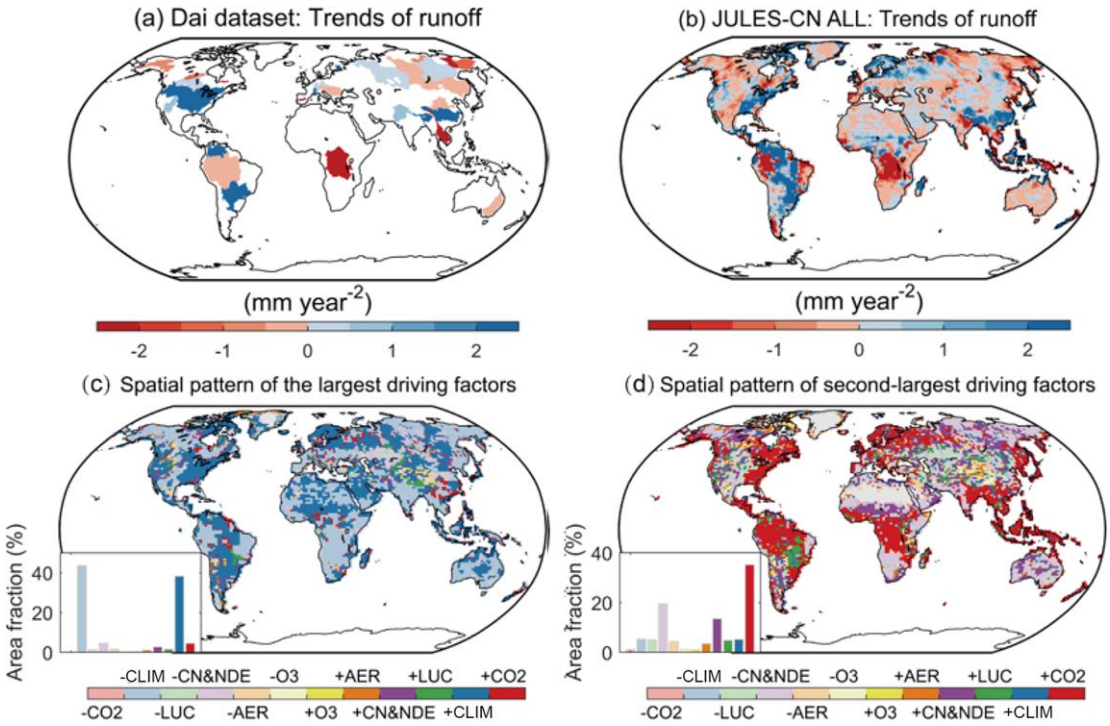

Figure 4. Drivers of runoff changes. Global patterns of trends in the river runoff from 1960 to 1999 from (a) Dai dataset (same as figure 2(a), different units) and from (b) JULES-CN model with all forcings ($CN_{CO2+CLIM+LUC+CN\&NDE+AER}$ simulation + O3 effects). (c) Spatial pattern of the factor with the largest absolute value of increasing (or decreasing) trends in runoff for each grid. The affecting factors include rising CO_2 (CO_2), climate change (CLIM), carbon–nitrogen interactions and nitrogen deposition (CN&NDE), land cover change (LUC), the diffuse radiation effects of aerosols (AER), and ozone concentration changes (O3). A prefix '+' of the driving factors indicates a positive effect on runoff trends, whereas '−' indicates a negative effect. (d) Spatial pattern of the factor with the absolute second-largest increasing (or decreasing) trends in runoff for each grid cell. Notations identical to (c). Panel insets in (c) and (d) are the fraction of vegetated area (%) that is dominantly driven by each factor. The colours of bars (insets) are identical to those used in the global maps.

may be different regionally, as suggested by figure 2(a), which shows not only spatial heterogeneity but also large differences in sign. We return to consider geographical differences, and find that at the local level, JULES-CN simulates a significant increase in runoff during the late twentieth century over eastern United States, northern Europe, some areas in China and a large area in South America. Decreased runoff is simulated over some areas of Canada, central Africa and west Amazon (figure 4(b)). These changes compare well to data (figures 2(a) and 4(a)).

For local runoff trends, multiple factors show much more diversity in their relative contributions to runoff changes. The driving factor of the largest magnitude and for each grid cell, as calculated by JULES-CN factorial simulations, is presented in figure 4(c). Figure 4(c) shows that unlike the mean dominant contributors to the global runoff trends, climate change is the factor responsible for the absolute largest trends of runoff. Climate as the dominant driver is for over 82% of global land area (excluding Antarctica), whereas rising atmospheric CO_2 concentration dominates runoff increases for <5% of global land area. For locations where climate change dominates, climate change impact on runoff is positive over 38% of global land area, and negative for the remaining 44%. For the remaining runoff increasing areas where climate is not the dominant driver, the main driving factor is either LUC or tropospheric ozone. This is especially notable for some regions in China and India (figure 4(c)). We also identify the factor with the second-largest absolute value of runoff trend, and observe this has strong geographical heterogeneity (figure 4(d)). Elevated CO_2 concentration, via its physiological effects, contributes to an upward trend in the runoff, and is the second-largest effect over 35% of global land area. In contrast, carbon–nitrogen interactions and nitrogen deposition induced the second-largest decreasing trends in runoff over the nitrogen-limited regions, e.g. Australia and the boreal regions at the high latitudes. LUC contributes to the second-largest runoff increase in west Amazon.

Actual trend values for different drivers are presented in figure 5. Trends in simulated runoff due to climate change, over the period 1960–1999, are shown in figure 5(a). The climate change signal (figure 5(a)) is predominantly a function of increasing atmospheric CO_2 concentration, which is the dominant driver when expressed via contribution to radiative forcing (IPCC 2013). Other smaller drivers are non-CO_2 greenhouse gases, volcano effects, solar fluctuations and atmospheric aerosols. Hence, figure 5(a) is regarded as broadly, an indirect CO_2 effect. Besides

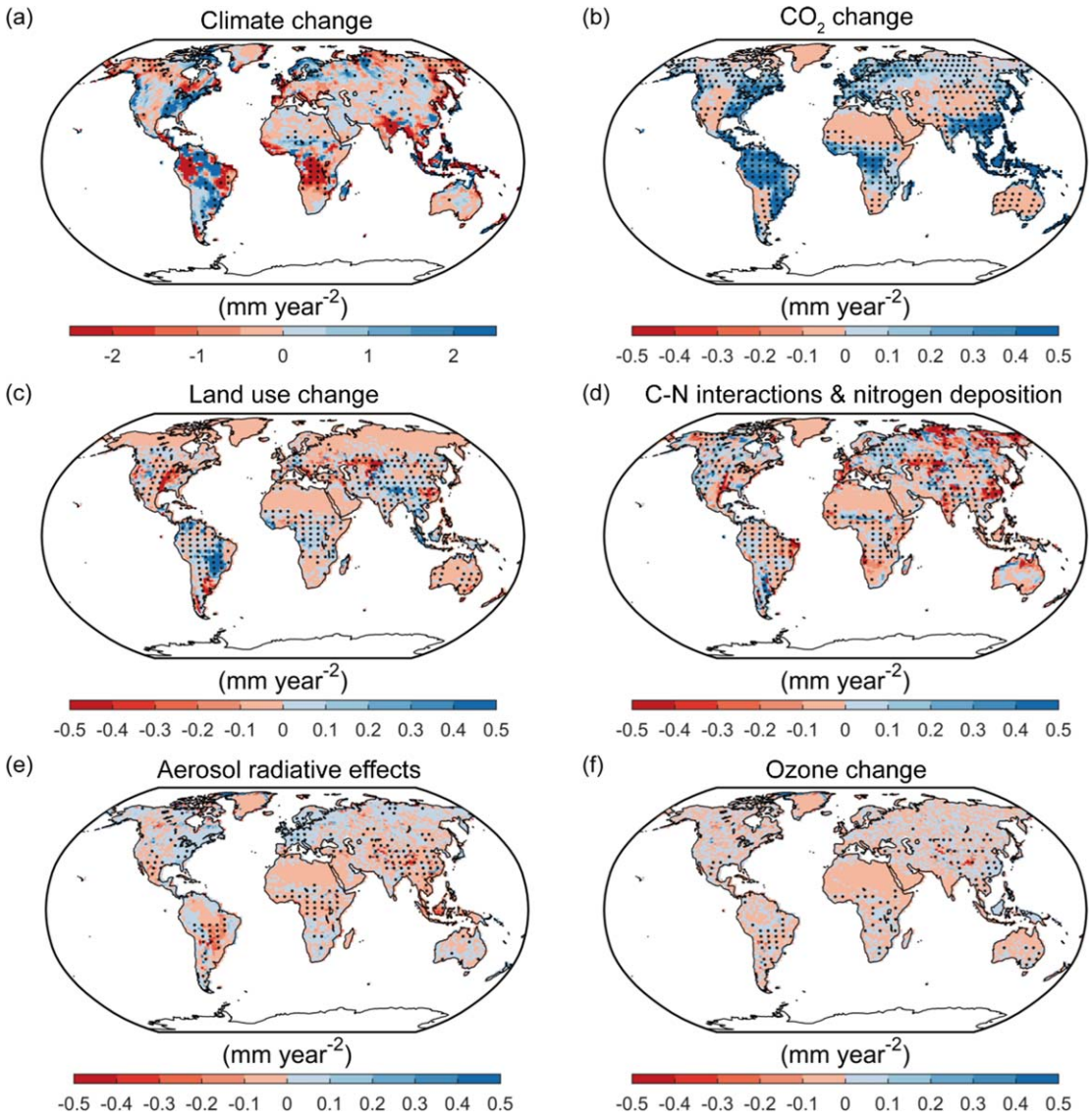

Figure 5. Global patterns of contributions of individual factors to modelled runoff trends over the period 1960–1999. Shown are (a) climate change ('CLIM'); (b) elevated atmospheric CO_2 concentration ('CO_2'); (c) land use change ('LUC'); (d) carbon–nitrogen interactions and nitrogen deposition ('CN & NDE'); (e) aerosol radiative effect ('AER'); (f) ozone change ('O3'). Stippling signifies that the linear trends at the local level are statistically significant at the 10% significance level.

temperature increases, rainfall intensity increases in some areas, wind speed changes affect near-surface turbulent exchange and surface conditions, which in turn can adjust evapotranspiration. This also causes an indirect effect, where the response to changed surface conditions alters land-atmosphere CO_2 exchange, and ultimately vegetation dynamics (McVicar *et al* 2012, Dourte *et al* 2015) (figure S3). However, the climate-induced runoff trends are correlated significantly with the trends of precipitation over 63% of global land area (figure S3), suggesting precipitation is the dominant local climate driver.

The net physiological and structural effects of vegetation response and impact on runoff, caused by rising atmospheric CO_2 concentration, is shown in figure 5(b). Higher CO_2 concentrations generally enhance runoff in humid regions, whereas it slightly reduces runoff in arid regions. For the wet regions, JULES-CN simulations suggest that runoff increases are related to mostly reductions in transpiration caused by CO_2-induced stomatal closure (figure S4(b) and text S1) reducing transpiration (figure S4(d)). In water-limited environments, the elevated CO_2 concentration reduces stomatal conductance instantaneously, through stomatal closure, to alleviate plant dryness stress. Howver, over longer time periods (e.g. decades), elevated CO_2 concentration leads to increased vegetation WUE, and which triggers increases in LAI and/or extended growing seasons. Such increases in LAI can enhance transpiration, through increased stomata density and number (figure S4(c)), which offset the retention effects of stomata closure (figure S4(d)). Additionally, higher LAI can raise canopy interception and related evaporation increases

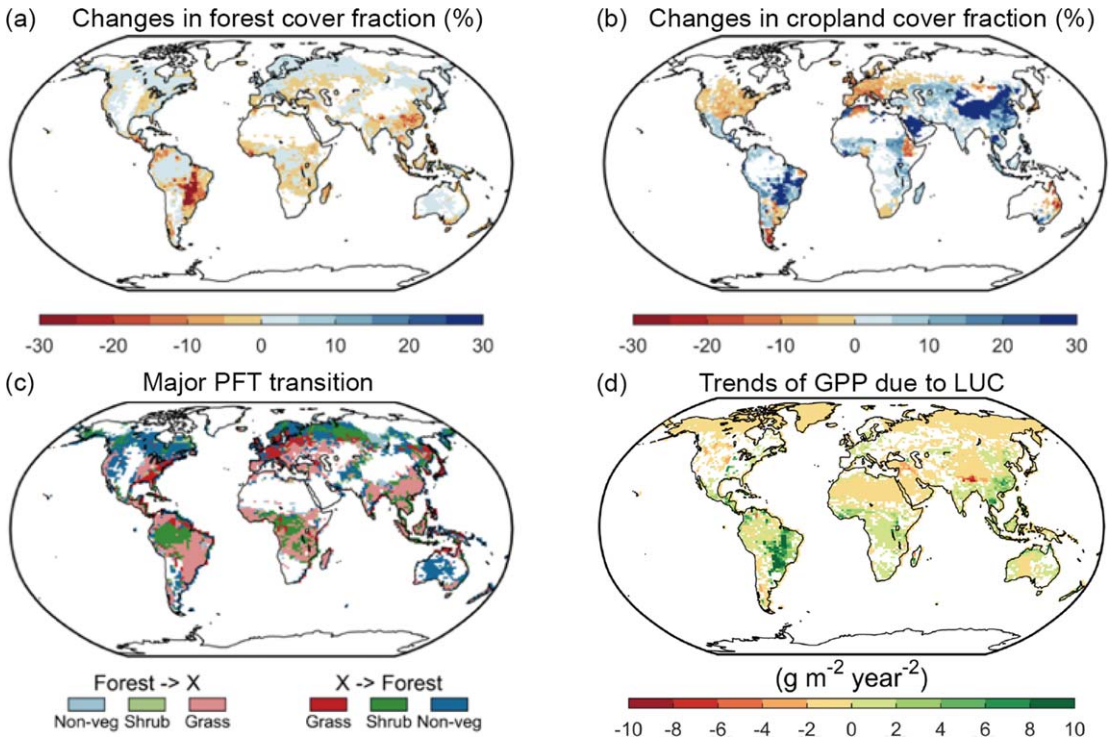

Figure 6. Spatial patterns of changes in the (a) forest and (b) cropland cover fractions for the period of 1960–1999. Panel (c) is the global Plant Function Type (PFT) transition maps for the same period. Cropland is referred to 'Grass' PFT in JULES-CN model. (d) Spatial patterns of contributions of land use change (LUC) to the modelled GPP trends over the period 1960–1999. White lands are omitted because linear trends of GPP are not significant.

(figure S4(f)). The balance of all of these effects in JULES is to lead to a slight decrease in runoff.

Figure 5(c) shows the impact of LUC, leading to runoff increases over the wet tropical regions (especially in the Amazonian region) and decreases in Southeast China, Central Asia, the eastern USA. The net losses of forest area (due to deforestation and/or fire; Klein Goldewijk *et al* 2011) and cropland expansion during the past four decades play multiple important roles. In the Amazonian region, simulations with JULES-CN model suggest that when forest is replaced by cropland (figures 6(a)–(c)), ET decreases, resulting in overall runoff increases, since compared to cropland (or grassland), forest has higher transpiration rates (Mahmood and Hubbard 2003). In contrast, the replacement of croplands in Southeast China is more productive than the replaced forest (figure 6(d)), leading to an increase in ET and a decrease in runoff. Also, runoff in Central Asia has decreased due to the local expansion of agriculture. Interestingly, in the eastern USA, a vegetation shift from C4 grasslands towards C3 grasslands has likely occurred (figures S5(c) and (d)). C3 grasslands have low WUE, which implies their ability to maintain photosynthesis depends on using more water, thus leading to decreased runoff.

Nitrogen availability limits plant growth, particularly over the temperate and boreal regions (LeBauer and Treseder 2008), potentially offset by raised nitrogen deposition. Explicitly modelling carbon–nitrogen interactions, JULES-CN simulations suggest that increased nitrogen deposition in Siberia, Middle East and southwest China results in increasing GPP, LAI and evapotranspiration, thereby decreasing runoff (figure 5(d)). However, in the Eastern Europe and North America, nitrogen limitation effects dominate, leading to decreasing leaf photosynthesis and transpiration, and thereby increasing runoff (figure S6).

Figure 5(e) shows that the impact of increases in aerosols in densely-populated and in biomass burning regions (figures S7(a) and (b)) during 1960–1999. This includes South America, central Africa, Australia, India, southern and western Asia. In contrast, most of south-west USA and western Europe experience aerosol decreases due to Clean Air policies. The upward trend of runoff in western Europe (except the Iberian Peninsula) and south-west US demonstrate the effect of diffuse radiation fraction (Mercado *et al* 2009 for details of diffuse fraction changes) decreases are larger than the opposing influence of total radiation increase. Raised atmospheric aerosol levels lead to diffuse fraction increases in South America, central Africa, Australia, India, southern and western Asia, which again dominant direct radiation changes. For these locations, this leads to increased transpiration and decreased runoff.

Finally, simulated changes in tropospheric ozone concentration over the study period leads to increased simulated runoff (figure 5(f)) with changes being statistically significantly over most of South America, Africa and southern China. Despite statistical

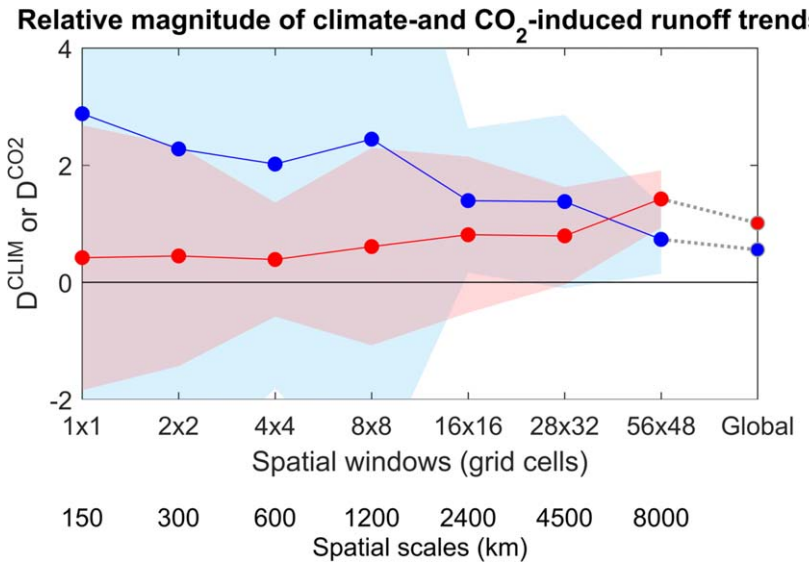

Figure 7. The relative magnitude of climate-induced and CO_2-induced runoff trends (i.e. D^{CLIM} and D^{CO2}) over different spatial scales of interest. This relative magnitude is calculated for spatial windows of $1 \times 1, 2 \times 2, 4 \times 4, 8 \times 8, 16 \times 16, 28 \times 32, 56 \times 48$ grid cells, and for all the grid cells over the globe. The longitudinal distance at 45°N is also marked along the *x*-axis for quantifying the magnitude of the spatial scales. Uncertainty bounds (given as shaded areas) refer to ± 1 standard deviations.

significance, the magnitude of runoff trends due to ozone changes is relatively small.

4. Discussion

4.1. Scale dependence of relative dominant factors

Investigated further is our finding that at the local scale, climate change is the dominant driver of runoff trends, whereas when integrated globally, the dominant factors are elevated CO_2 concentration and LUC. We explore whether compensatory effects of climate change when scaling from local to global scales explain this paradox. The calculated relative magnitude of climate-induced runoff trend (D^{CLIM}) decreases with increasing spatial aggregation, while the relative magnitude of CO_2-induced runoff trend (D^{CO2}) increases (figure 7). The decreases in D^{CLIM} is due to a compensation of positive and negative trends of climate-induced runoff between different grid cells (as shown in figure 5(a)), whereas the CO_2-induced runoff trends are generally universal and positive (figure 5(b)). This strong dependence of main driver on scale has similarities to findings by Jung *et al* (2017), but with their analysis in terms of land-atmosphere CO_2 exchanges.

4.2. The influence of elevated CO_2 concentration and N-cycle interactions

As outlined above, rising atmospheric CO_2 concentration influences plants and associated water cycle in two contrasting ways. First, the CO_2 fertilization effect changes vegetation structure, stimulates photosynthesis and raises the biomass of C3 plants. This first effect has three consequences: (i) it increases transpiration by raising the number of stomata due to increased LAI; (ii) it increases canopy interception loss due to raised LAI and (iii) soil evaporation decreases due to reduced available energy at the surface. Such changes reduce local runoff. Second, there is the direct physiological effect, causing stomatal closure, (although higher WUE), leading to transpiration decrease and runoff increase. JULES-CN calculate the balance between these two-opposing effect is such that runoff in drylands has decreased, but in wet regions it has increased. Gerten *et al* (2008) performed a similar analysis with the LPJmL model, which is a C-only model. They found rising atmospheric CO_2 levels decreased runoff in some drylands and increased runoff in temperate and boreal regions, which is consistent with JULES-CN. However, LPJmL simulated non-significant trends in runoff over the tropics, which are smaller changes than we predict. Using the ORCHIDEE model (C-only model), Piao *et al* (2007) found the net effect of CO_2 on runoff to be overwhelmed by CO_2 fertilization effects (i.e. rather than direct stomata closure effects), and so negative across tropical wet and temperate regions, and thus different to our findings. In addition, using 13 land surface models, Mao *et al* (2015) found at elevated CO_2, for most areas and especially these regions covered by tropical broadleaf evergreen trees and high latitude shrubs, showed decreasing trends in evapotranspiration, whereas dry areas with sparse vegetation showed increasing evaporation. This result is consistent with our findings, since runoff often changes in opposite directions to evapotranspiration (since runoff is equal to precipitation minus evapotranspiration and precipitation shows relatively little change for altered CO_2).

In addition to the uncertainty associated with direct and indirect CO_2 influences, until recently land surface models have lacked representation of the terrestrial carbon–nitrogen cycle. Terrestrial carbon uptake is modelled as limited by the availability of nitrogen in JULES-CN

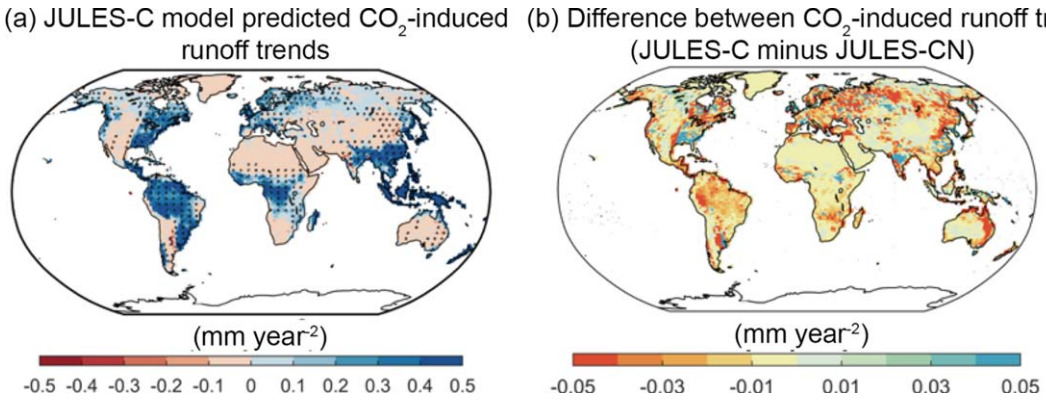

Figure 8. The influence of elevated CO_2 concentration on runoff and N-cycle interactions from the JULES model. (a) Global patterns of modelled runoff trends due to elevated atmospheric CO_2 concentration derived from JULES-C model. Black dots denote where the trends are statistically significant at the 10% level. (b) Global patterns of differences in CO_2-induced runoff trends between JULES-C model (without carbon–nitrogen interactions; figure 8(a)) and JULES-CN model (with carbon–nitrogen interactions; figure 5(b)).

simulation. Specifically, an ecosystem becomes limited when insufficient nitrogen is available for plants to allocate net photosynthetic to growth, in which case photosynthesis is 'downregulated' to match the available inorganic nitrogen. Nitrogen does not directly affect photosynthetic capacity through leaf nitrogen concentrations, but instead acts indirectly by controlling the biomass and LAI. An increase in nitrogen limitation would generally act to suppress the evaporative fraction and vice versa for a decrease in limitation. In other words, CO_2 fertilization is known to be constrained by nitrogen availability (Felzer *et al* 2009, Norby *et al* 2010, Zaehle 2013), and therefore models without a coupled C and N cycle may overestimate fertilization-related runoff decreases (Hungate *et al* 2003, Zaehle and Dalmonech 2011). We compare projections of runoff from JULES-CN (i.e. with carbon–nitrogen interaction processes) and JULES-C model (without carbon–nitrogen interaction processes). We find JULES-C projects a weaker increase in CO_2-induced runoff trends over most regions of the world, especially for boreal forest regions, compared to the JULES-CN model (figure 8(b)). This is expected, as JULES-C model projects larger CO_2 fertilization-induced runoff decreases, which offsets more runoff increases due to raised stomatal closure. Comparison of figures 8(a) and (b) shows the relative importance of the inclusion of the N-cycle on runoff. We note that our results are specific to the JULES model. We hope our analysis will act as an incentive for other DGVM groups, to determine the impact of new geochemical cycle modelling (and especially the nitrogen dynamics) on land impacts of concern, and in particular runoff.

Our projections do have caveats. Our simulations are in 'offline' mode (forced by reanalysis data), hence lacking any land-atmosphere feedbacks in response to changes in land surface configuration (Smith *et al* 2016); this might modulate future predictions of runoff. Uncertainty remains in representation of several eco-hydrological processes, and including stomatal conductance-photosynthesis coupling and the transpiration response of plants (De Kauwe *et al* 2013, Swann *et al* 2016). Land models are known to exhibit strong differences and biases in their aggregation from leaf to full canopy fluxes (Lian *et al* 2018).

5. Conclusion

We study spatial and temporal variations in runoff at global and local scales during the period 1960–1999. Our advances here are using a land surface model with explicit accounting for nitrogen dynamics, which allows assessment of the effect that this geochemical cycle has on spatial and temporal variations in runoff at global and local scales. We find the JULES-CN model performs well in comparison to measurements, and this provides some confidence in the subsequent factorial analysis of individual drivers. At the global scale, changing runoff has been mainly a consequence of rising CO_2 concentration. Rising atmospheric CO_2 concentration and LUC make positive contributions to global runoff changes, of $+0.18\ mm\ yr^{-2}$ and $+0.05\ mm\ yr^{-2}$ respectively. In contrast, carbon–nitrogen interactions and nitrogen deposition make negative contributions to the global mean runoff trend ($-0.03\ mm\ yr^{-2}$). The relative roles of aerosol deposition and tropospheric ozone changes are small.

Locally, however, our simulations show the multiple factors instead cause much more diverse contributions to river runoff changes. Climate change is the factor with the absolute largest trends of runoff, covering over 82% of global land area. Note that as the climate change signal is predominantly triggered by increasing atmospheric CO_2 concentration, the effect of climate change on runoff can be considered as an indirect effect of raised CO_2 concentrations. We can explain the shift of the dominant control for runoff change from climate change at the local scale to the direct effect of the rising CO_2 concentration at the global scale. Such scale dependence is due to temporal climate-driven runoff variations compensating as spatial length scales increase. This finding confirms that climate variation not only forces runoff changes locally but

additionally and perhaps more importantly, the spatial covariation of climate variables makes the integrated global hydrological response different. This has similarities to the scale-dependent findings of Jung *et al* (2017), although their analysis is in the context of atmosphere-land CO_2 exchange. Despite some drivers having relatively small impacts globally, spatial variation leads to the conclusion that the roles of non-climatic factors, including nitrogen deposition and interactions, LUC, aerosol and ozone changes, must be including when projecting local future changes in the water cycle and climate. Additional drivers, such as direct human intervention (e.g. dams, irrigation) and permafrost process, need routine inclusion in land surface models. We hope that extension occurs for the datasets used in this study, to test if the noted emerging signals have continued during the last two decades. With longer datasets, formal detection and attribution analyses (Allen and Stott 2003) may become possible, enabling deeper understanding of the amplitude of changes induced by each factor, as reflected in observations.

Acknowledgments

We acknowledge NERC National Capability Funding. HY recognizes support from the CSC scholarship, funding a 12 month visit to the UK Centre for Ecology and Hydrology. CH thanks the Newton program CSSP-China for support. LM and SS were supported by the Newton Fund through the Met Office Climate Science for Service Partnership Brazil (CSSP Brazil). The contribution of LM was also supported through the UK Natural Environment Research council through The UK Earth System Modelling Project (UKESM, Grant No. NE/N017951/1).

Data availability statement

The model data that support the findings of this study and the Matlab code are available from the corresponding author upon reasonable request.

ORCID iDs

Hui Yang https://orcid.org/0000-0001-6454-8954
Chris Huntingford https://orcid.org/0000-0002-5941-7770

References

Allen M R and Stott P A 2003 Estimating signal amplitudes in optimal fingerprinting: I *Theory. Clim. Dyn.* **21** 477–91

Bellouin N, Boucher O, Haywood J, Johnson C, Jones A, Rae J and Woodward S 2007 Improved representation of aerosols for $HadGEM_2$ *Hadley Cent. Tech. Note* **73** 43

Berghuijs W R, Woods R A and Hrachowitz M 2014 A precipitation shift from snow towards rain leads to a decrease in streamflow *Nat. Clim. Change* **4** 583–6

Best M J *et al* 2011 The joint uk land environment simulator (JULES), model description: I. Energy and water fluxes *Geosci. Model Dev.* **4** 677–99

Blyth E, Clark D B, Ellis R, Huntingford C, Los S, Pryor M, Best M and Sitch S 2011 A comprehensive set of benchmark tests for a land surface model of simultaneous fluxes of water and carbon at both the global and seasonal scale *Geosci. Model Dev.* **4** 255–69

Bureau C S 2000 *China Statistical Yearbook* vol 10 (Beijing: China Statistical Bureau) p 33

Clark D B *et al* 2011 The Joint UK land environment simulator (JULES), model description: II. Carbon fluxes and vegetation dynamics *Geosci. Model Dev.* **4** 701–22

Cox P M, Betts R A, Bunton C B, Essery R L H, Rowntree P R and Smith J 1999 The impact of new land surface physics on the GCM simulation of climate and climate sensitivity *Clim. Dyn.* **15** 183–203

Cox P M, Huntingford C and Harding R J 1998 A canopy conductance and photosynthesis model for use in a GCM land surface scheme *J. Hydrol.* **212** 79–94

Dai A, Qian T, Trenberth K E and Milliman J D 2009 Changes in continental freshwater discharge from 1948 to 2004 *J. Clim.* **22** 2773–92

De Kauwe M G *et al* 2013 Forest water use and water use efficiency at elevated CO_2: a model-data intercomparison at two contrasting temperate forest FACE sites *Glob. Change Biol.* **19** 1759–79

Dourte D R, Fraisse C W and Bartels W L 2015 Exploring changes in rainfall intensity and seasonal variability in the Southeastern US: Stakeholder engagement, observations, and adaptation *Clim. Risk Manage.* **7** 11–9

Essery R L H, Best M J, Betts R A, Cox P M and Taylor C M 2003 Explicit representation of subgrid heterogeneity in a GCM land surface scheme *J. Hydrometeorol.* **4** 530–43

Felzer B S, Cronin T W, Melillo J M, Kicklighter D W and Schlosser C A 2009 Importance of carbon-nitrogen interactions and ozone on ecosystem hydrology during the 21st century *J. Geophys. Res. Biogeosci.* **114** G01020

Gedney N, Cox P M, Betts R A, Boucher O, Huntingford C and Stott P A 2006 Detection of a direct carbon dioxide effect in continental river runoff records *Nature* **439** 835–8

Gedney N, Huntingford C, Weedon G P, Bellouin N, Boucher O and Cox P M 2014 Detection of solar dimming and brightening effects on Northern Hemisphere river flow *Nat. Geosci.* **7** 796–800

Gerten D, Rost S, von Bloh W and Lucht W 2008 Causes of change in 20th century global river discharge *Geophys. Res. Lett.* **35** L20405

Haddeland I *et al* 2014 Global water resources affected by human interventions and climate change *Proc. Natl Acad. Sci. USA* **111** 3251–6

Hungate B A, Dukes J S, Shaw M R, Luo Y and Field C B 2003 Nitrogen and climate change *Science* **302** 1512–3

Huntingford C, Cox P M, Mercado L M, Sitch S, Bellouin N, Boucher O and Gedney N 2011 Highly contrasting effects of different climate forcing agents on terrestrial ecosystem services *Phil. Trans. R. Soc.* A **369** 2026–37

Huntington T G 2006 Evidence for intensification of the global water cycle: review and synthesis *J. Hydrol.* **319** 83–95

IPCC 2013 *Climate Change 2013: The Physical Science Basis. Contribution of Working Group I to the Fifth Assessment Report of the Intergovernmental Panel on Climate Change* ed T F Stocker *et al* (Cambridge and New York, NY: Cambridge University Press)

Jiménez Cisneros B E, Oki T, Arnell N W, Benito G, Cogley J G, Döll P, Jiang T and Mwakalila S S 2014 Freshwater resources *Climate Change 2014: Impacts, Adaptation, and Vulnerability Contribution of Working Group II to the Fifth Assessment Report of the Intergovernmental Panel on Climate Change* ed C B Field *et al* (Cambridge and New York, NY: Cambridge University Press) pp 229–69

Jung M *et al* 2017 Compensatory water effects link yearly global land CO_2 sink changes to temperature *Nature* **541** 516–20

Keeling C D and Whorf T P 2005 Atmospheric CO_2 records from sites in the SIO air sampling network *Trends: A Compendium of Data on Global Change* pp 16–26

Klein Goldewijk K, Beusen A, Van Drecht G and De Vos M 2011 The HYDE 3.1 spatially explicit database of human-induced global land-use change over the past 12,000 years *Glob. Ecol. Biogeogr.* **20** 73–86

Lamarque J F *et al* 2013 Multi-model mean nitrogen and sulfur deposition from the atmospheric chemistry and climate model intercomparison project (ACCMIP): evaluation of historical and projected future *Atmos. Chem. Phys.* **13** 7997–8018

LeBauer D S and Treseder K K 2008 Nitrogen limitation of net primary productivity in terrestrial ecosystems is globally distributed *Ecology* **89** 371–9

Lian X *et al* 2018 Partitioning global land evapotranspiration using CMIP5 models constrained by observations *Nat. Clim. Change* **8** 640–6

Lombardozzi D L, Bonan G B, Smith N G, Dukes J S and Fisher R A 2015 Temperature acclimation of photosynthesis and respiration: a key uncertainty in the carbon cycle-climate feedback *Geophys. Res. Lett.* **42** 8624–31

Mahmood R and Hubbard K G 2003 Simulating sensitivity of soil moisture and evapotranspiration under heterogeneous soils and land uses *J. Hydrol.* **280** 72–90

Mao J *et al* 2015 Disentangling climatic and anthropogenic controls on global terrestrial evapotranspiration trends *Environ. Res. Lett.* **10** 094008

McVicar T R *et al* 2012 Global review and synthesis of trends in observed terrestrial near-surface wind speeds: Implications for evaporation *J. Hydrol.* **416** 182–205

Mercado L M, Bellouin N, Sitch S, Boucher O, Huntingford C, Wild M and Cox P M 2009 Impact of changes in diffuse radiation on the global land carbon sink *Nature* **458** 1014–1018.

Mercado L M, Huntingford C, Gash J H, Cox P M and Jogireddy V 2007 Improving the representation of radiation interception and photosynthesis for climate model applications *Tellus* B **59** 553–65

Mills G, Harmens H, Wagg S, Sharps K, Hayes F, Fowler D, Sutton M and Davies B 2016 Ozone impacts on vegetation in a nitrogen enriched and changing climate *Environ. Pollut.* **208** 898–908

Milly P C D, Dunne K A and Vecchia A V 2005 Global pattern of trends in streamflow and water availability in a changing climate *Nature* **438** 347–50

Norby R J, Warren J M, Iversen C M, Medlyn B E and McMurtrie R E 2010 CO_2 enhancement of forest productivity constrained by limited nitrogen availability *Proc. Natl Acad. Sci. USA* **107** 19368–73

Ohmura A and Wild M 2002 Is the hydrological cycle accelerating? *Science* **298** 1345–6

Oki T and Kanae S 2006 Global hydrological cycles and world water resources *Science* **313** 1068–72

Oliver R J, Mercado L M, Sitch S, Simpson D, Medlyn B E, Lin Y S and Folberth G A 2018 Large but decreasing effect of ozone on the European carbon sink *Biogeosciences* **15** 4245–69

Pavelsky T M and Laurence C S 2006 Intercomparison of four global precipitation data sets and their correlation with increased Eurasian river discharge to the Arctic Ocean *J. Geophys. Res. Atmos.* **111** D21

Piao S, Friedlingstein P, Ciais P, de Noblet-Ducoudré N, Labat D and Zaehle S 2007 Changes in climate and land use have a larger direct impact than rising CO_2 on global river runoff trends *Proc. Natl Acad. Sci. USA* **104** 15242–7

Le Quéré C *et al* 2012 The global carbon budget 1959–2011 *Earth Syst. Sci. Data* **5** 165–85

Sanderson M G, Jones C D, Collins W J, Johnson C E and Derwent R G 2003 Effect of climate change on isoprene emissions and surface ozone levels *Geophys. Res. Lett.* **30** 1936

Shi X, Mao J, Thornton P E, Hoffman F M and Post W M 2011 The impact of climate, CO_2, nitrogen deposition and land use change on simulated contemporary global river flow *Geophys. Res. Lett.* **38** L08704

Sitch S, Cox P M, Collins W J and Huntingford C 2007 Indirect radiative forcing of climate change through ozone effects on the land-carbon sink *Nature* **448** 791–4

Smith W K, Reed S C, Cleveland C C, Ballantyne A P, Anderegg W R, Wieder W R, Liu Y Y and Running S W 2016 Large divergence of satellite and Earth system model estimates of global terrestrial CO_2 fertilization *Nat. Clim. Change* **6** 306–12

Swann A L, Hoffman F M, Koven C D and Randerson J T 2016 Plant responses to increasing CO_2 reduce estimates of climate impacts on drought severity *Proc. Natl Acad. Sci. USA* **113** 10019–24

Tang Q, Oki T, Kanae S and Hu H 2007 The influence of precipitation variability and partial irrigation within grid cells on a hydrological simulation *J. Hydrometeorol.* **8** 499–512

Wiltshire A *et al* 2019 JULES-CN: a coupled Carbon-Nitrogen Scheme (JULES vn4.7) *in prep*

Xue J and Gavin K 2008 Effect of rainfall intensity on infiltration into partly saturated slopes *Geotech. Geol. Eng.* **26** 199–209

Yang H, Piao S, Huntingford C, Ciais P, Li Y, Wang T, Peng S, Yang Y, Yang D and Chang J 2018 Changing the retention properties of catchments and their influence on runoff under climate change *Environ. Res. Lett.* **13** 094019

Yang H, Zhou F, Piao S, Huang M, Chen A, Ciais P, Li Y, Lian X and Zeng Z 2017 Regional patterns of future runoff changes from Earth system models constrained by observation *Geophys. Res. Lett.* **44** 5540–9

Zaehle S 2013 Terrestrial nitrogen-carbon cycle interactions at the global scale *Phil. Trans. R. Soc.* B **368** 20130125

Zaehle S and Dalmonech D 2011 Carbon-nitrogen interactions on land at global scales: current understanding in modelling climate biosphere feedbacks *Curr. Opin. Environ. Sustain.* **3** 311–20

Zulkafli Z, Buytaert W, Onof C, Lavado W and Guyot J L 2013 A critical assessment of the JULES land surface model hydrology for humid tropical environments *Hydrol. Earth Syst. Sci.* **17** 1113–32